



HAL
open science

Search for anomalous couplings in the Higgs sector at LEP

P. Achard, O. Adriani, M. Aguilar-Benitez, J. Alcaraz, G. Alemanni, J. Allaby, A. Aloisio, M.G. Alviggi, H. Anderhub, V.P. Andreev, et al.

► **To cite this version:**

P. Achard, O. Adriani, M. Aguilar-Benitez, J. Alcaraz, G. Alemanni, et al. Search for anomalous couplings in the Higgs sector at LEP. *Physics Letters B*, 2004, 589, pp.89-102. 10.1016/j.physletb.2004.03.048 . in2p3-00021833

HAL Id: in2p3-00021833

<https://in2p3.hal.science/in2p3-00021833v1>

Submitted on 19 May 2004

HAL is a multi-disciplinary open access archive for the deposit and dissemination of scientific research documents, whether they are published or not. The documents may come from teaching and research institutions in France or abroad, or from public or private research centers.

L'archive ouverte pluridisciplinaire **HAL**, est destinée au dépôt et à la diffusion de documents scientifiques de niveau recherche, publiés ou non, émanant des établissements d'enseignement et de recherche français ou étrangers, des laboratoires publics ou privés.

Search for Anomalous Couplings in the Higgs Sector at LEP

The L3 Collaboration

Abstract

Anomalous couplings of the Higgs boson are searched for through the processes $e^+e^- \rightarrow H\gamma$, $e^+e^- \rightarrow e^+e^-H$ and $e^+e^- \rightarrow HZ$. The mass range $70 \text{ GeV} < m_H < 190 \text{ GeV}$ is explored using 602 pb^{-1} of integrated luminosity collected with the L3 detector at LEP at centre-of-mass energies $\sqrt{s} = 189 - 209 \text{ GeV}$. The Higgs decay channels $H \rightarrow f\bar{f}$, $H \rightarrow \gamma\gamma$, $H \rightarrow Z\gamma$ and $H \rightarrow WW^{(*)}$ are considered and no evidence is found for anomalous Higgs production or decay. Limits on the anomalous couplings d , d_B , Δg_1^Z , $\Delta\kappa_\gamma$ and ξ^2 are derived as well as limits on the $H \rightarrow \gamma\gamma$ and $H \rightarrow Z\gamma$ decay rates.

Submitted to *Phys. Lett. B*

1 Introduction

The mechanism of spontaneous symmetry breaking is a cornerstone of the Standard Model of the electroweak interactions [1]. It explains the observed masses of the elementary particles and postulates an additional particle, the Higgs boson. Despite its relevance, experimental information on the Higgs boson is scarce and indirect. It leaves room for deviations from the Standard Model expectations such as anomalous couplings of the Higgs boson.

The Standard Model can be extended, via a linear representation of the $SU(2)_L \times U(1)_Y$ symmetry breaking mechanism [2], to higher orders where new interactions between the Higgs boson and gauge bosons become possible. These modify the production mechanisms and decay properties of the Higgs boson. The relevant CP-invariant Lagrangian terms are [3]:

$$\begin{aligned} \mathcal{L}_{\text{eff}} = & g_{H\gamma\gamma} H A_{\mu\nu} A^{\mu\nu} + g_{HZ\gamma}^{(1)} A_{\mu\nu} Z^\mu \partial^\nu H + g_{HZ\gamma}^{(2)} H A_{\mu\nu} Z^{\mu\nu} \\ & + g_{HZZ}^{(1)} Z_{\mu\nu} Z^\mu \partial^\nu H + g_{HZZ}^{(2)} H Z_{\mu\nu} Z^{\mu\nu} + g_{HZZ}^{(3)} H Z_\mu Z^\mu \\ & + g_{HWW}^{(1)} (W_{\mu\nu}^+ W_-^\mu \partial^\nu H + h.c.) + g_{HWW}^{(2)} H W_{\mu\nu}^+ W_-^{\mu\nu}, \end{aligned} \quad (1)$$

where A_μ , Z_μ , W_μ and H are the photon, Z, W and Higgs fields, respectively, and $X_{\mu\nu} = \partial_\mu X_\nu - \partial_\nu X_\mu$. The couplings in this Lagrangian are parametrized as [4–6]:

$$g_{H\gamma\gamma} = \frac{g}{2m_W} (d \sin^2\theta_W + d_B \cos^2\theta_W) \quad (2)$$

$$g_{HZ\gamma}^{(1)} = \frac{g}{m_W} (\Delta g_1^Z \sin 2\theta_W - \Delta\kappa_\gamma \tan\theta_W) \quad (3)$$

$$g_{HZ\gamma}^{(2)} = \frac{g}{2m_W} \sin 2\theta_W (d - d_B) \quad (4)$$

$$g_{HZZ}^{(1)} = \frac{g}{m_W} (\Delta g_1^Z \cos 2\theta_W + \Delta\kappa_\gamma \tan^2\theta_W) \quad (5)$$

$$g_{HZZ}^{(2)} = \frac{g}{2m_W} (d \cos^2\theta_W + d_B \sin^2\theta_W) \quad (6)$$

$$g_{HZZ}^{(3)} = \frac{g m_W}{2 \cos^2\theta_W} \delta_Z \quad (7)$$

$$g_{HWW}^{(1)} = \frac{g m_W}{m_Z^2} \Delta g_1^Z \quad (8)$$

$$g_{HWW}^{(2)} = \frac{g}{m_W} \frac{d}{\cos 2\theta_W}, \quad (9)$$

where g is the $SU(2)_L$ coupling constant, θ_W is the weak mixing angle and m_W and m_Z represent the masses of the W and Z bosons, respectively. The five dimensionless parameters d , d_B , Δg_1^Z , $\Delta\kappa_\gamma$ and δ_Z constitute a convenient set to describe deviations in the interactions between the Higgs boson and gauge bosons. They are not severely constrained by electroweak measurements at the Z pole or at lower energies [3, 7].

The couplings d and d_B were introduced in Reference 4, while Δg_1^Z and $\Delta\kappa_\gamma$ also describe possible deviations in the couplings of W bosons with photons and Z bosons [5]. A search for anomalous Higgs production and decay with non-vanishing values of Δg_1^Z or $\Delta\kappa_\gamma$ is a complementary study to the analysis of triple-gauge-boson couplings in the $e^+e^- \rightarrow W^+W^-$ process. The parameter $\xi^2 = (1 + \delta_Z)^2$ describes a global rescaling of all Higgs couplings and affects the Higgs production cross section, but not its branching fractions [6].

We search for a Higgs particle produced in the $e^+e^- \rightarrow H\gamma$ and $e^+e^- \rightarrow e^+e^-H$ processes shown in Figures 1a and 1b. Their rates would be enhanced in presence of anomalous $H\gamma\gamma$ and

HZ γ couplings. These processes probe Higgs masses, m_H , up to the centre-of-mass energy of the collision, \sqrt{s} . For $m_H < \sqrt{s} - m_Z$, this analysis is complemented by the results from the L3 searches for the $e^+e^- \rightarrow HZ$ process [8, 9], which are sensitive to anomalous HZZ and HZ γ couplings, as shown in Figure 1c.

The existence of $H\gamma\gamma$ and HZ γ couplings would lead to large $H \rightarrow \gamma\gamma$ and $H \rightarrow Z\gamma$ branching fractions, which at tree level are zero in the Standard Model. These decay modes have complementary sensitivities and allow to probe a large part of the parameter space. In addition, the decay $H \rightarrow WW^{(*)}$ would also be enhanced in the presence of anomalous HWW couplings.

The data used in this analysis were collected with the L3 detector [10] at LEP at $\sqrt{s} = 189 - 209$ GeV and correspond to an integrated luminosity of 602 pb^{-1} . Searches for anomalous Higgs production were previously performed, with data of lower energy and integrated luminosity, by L3 and other experiments [11, 12]. Other non-standard Higgs searches performed at LEP are reported in [9, 13]. The results reported in this Letter include and supersede those of Reference 11.

2 Analysis strategy

Table 1 summarizes the experimental signatures considered for the study of Higgs anomalous couplings according to the different production mechanisms and decay channels.

For the $e^+e^- \rightarrow H\gamma$ process, the decay channels $H \rightarrow \gamma\gamma$, $H \rightarrow Z\gamma$ and $H \rightarrow WW^{(*)}$ are investigated. Only hadronic decays of Z and W bosons are considered.

For the $e^+e^- \rightarrow e^+e^-H$ process, only the $H \rightarrow \gamma\gamma$ decay is studied. The $H \rightarrow b\bar{b}$ decay was considered in the study of the $e^+e^- \rightarrow e^+e^-H$ and $e^+e^- \rightarrow H\gamma$ processes for data collected at $\sqrt{s} = 189$ GeV [11]. This decay is dominant for $m_H \lesssim m_Z$, where $H \rightarrow \gamma\gamma$ is strongly suppressed and $H \rightarrow Z\gamma$ is kinematically forbidden. At the centre-of-mass energies considered in this Letter, this region is efficiently covered by an interpretation of the results of the search for the $e^+e^- \rightarrow HZ$ process [8] and the $H \rightarrow b\bar{b}$ decay is not considered here.

No dedicated selection is devised for the $e^+e^- \rightarrow HZ$ process and the limits obtained by L3 in the searches for the Standard Model Higgs boson and for a fermiophobic Higgs boson are interpreted in terms of anomalous Higgs couplings.

The analysis is performed as a function of m_H in steps of 1 GeV. The $H \rightarrow \gamma\gamma$, $H \rightarrow Z\gamma$ and $H \rightarrow WW^{(*)}$ decays probe the ranges $70 \text{ GeV} < m_H < 190 \text{ GeV}$, $95 \text{ GeV} < m_H < 190 \text{ GeV}$ and $130 \text{ GeV} < m_H < 190 \text{ GeV}$, respectively.

After the event selections described below, variables which depend on m_H are built to discriminate signal and background. Finally, the number of events in a mass window around the m_H value under study is compared with the Standard Model expectation and interpreted in terms of cross sections and anomalous couplings.

3 Data and Monte Carlo samples

Table 2 lists the centre-of-mass energies and the corresponding integrated luminosities used in this analysis. The data at $\sqrt{s} = 189$ GeV are re-analysed for the $e^+e^- \rightarrow H\gamma \rightarrow \gamma\gamma\gamma$ and $e^+e^- \rightarrow e^+e^-H \rightarrow e^+e^-\gamma\gamma$ channels and results for the full range $\sqrt{s} = 189 - 209$ GeV are reported here. All other analyses discussed in this Letter refer to the $\sqrt{s} = 192 - 209$ GeV range, and their results are then combined with those obtained at $\sqrt{s} = 189$ GeV [11].

To describe the $e^+e^- \rightarrow H\gamma$ process we wrote a Monte Carlo generator which assumes a $1 + \cos^2 \theta_H$ dependence of the differential cross section as a function of the cosine of the Higgs production angle, θ_H . It includes effects of initial-state [14] and final-state [15] radiation as well as spin correlations and off-shell contributions in cascade decays such as $H \rightarrow Z\gamma \rightarrow f\bar{f}\gamma$.

The $e^+e^- \rightarrow e^+e^-H$ process is interpreted as the production of a narrow-width spin-zero resonance in two-photon collisions, and modelled with the PC Monte Carlo generator [16].

The differential cross section of the process $e^+e^- \rightarrow HZ$ in the presence of anomalous couplings is taken from Reference 17. References 18 and 19 are used for the branching fractions and partial widths of a Higgs boson with anomalous couplings. The interference between the $e^+e^- \rightarrow HZ$ process in the Standard Model and in presence of anomalous couplings [17] is taken into account in the simulation. It is negligible for the $e^+e^- \rightarrow H\gamma$ and $e^+e^- \rightarrow e^+e^-H$ cases.

Signal events are generated for $70 \text{ GeV} < m_H < 190 \text{ GeV}$, in steps of 20 GeV. More than 5000 signal events are generated for each value of m_H and for each process under study. For intermediate values of the Higgs mass, the signal efficiency is interpolated between the generated values.

Standard Model processes are modelled with the following Monte Carlo generators: GGG [20] for $e^+e^- \rightarrow \gamma\gamma(\gamma)$, KK2f [21] for $e^+e^- \rightarrow q\bar{q}(\gamma)$, PYTHIA [22] for $e^+e^- \rightarrow ZZ$ and $e^+e^- \rightarrow Ze^+e^-$, KORALW [23] for $e^+e^- \rightarrow W^+W^-(\gamma)$ and EXCALIBUR [24] for $e^+e^- \rightarrow We\nu$ and other four-fermion final states.

The L3 detector response is simulated using the GEANT program [25] which takes into account effects of energy loss, multiple scattering and showering in the detector. Time-dependent detector inefficiencies, as monitored during the data-taking period, are included in the simulations.

4 Event selection

All analyses presented in this Letter rely on photon identification. Photon candidates are defined as clusters in the electromagnetic calorimeter with a shower profile consistent with that of a photon and no associated track in the tracking chamber. To reduce contributions from initial-state and final-state radiation, photon candidates must satisfy $E_\gamma > 5 \text{ GeV}$ and $|\cos \theta_\gamma| < 0.97$, where E_γ is the photon energy and θ_γ its polar angle.

Events with hadronic decays of the Z and W bosons in the $H \rightarrow Z\gamma$ and $H \rightarrow WW^{(*)}$ channels are pre-selected requiring high particle multiplicity and a visible energy, E_{vis} , satisfying $0.8 < E_{vis}/\sqrt{s} < 1.2$.

4.1 The $e^+e^- \rightarrow H\gamma \rightarrow \gamma\gamma\gamma$ analysis

Events from the $e^+e^- \rightarrow H\gamma \rightarrow \gamma\gamma\gamma$ process are selected by requiring three photon candidates in the central region of the detector, $|\cos \theta_\gamma| < 0.8$, with a total electromagnetic energy larger than $\sqrt{s}/2$. Out of the three possible two-photon combinations, the one with a mass, $m_{\gamma\gamma}$, closest to the m_H hypothesis under investigation is retained. As an example, Figure 2a presents the distribution of $m_{\gamma\gamma}$ for $m_H = 110 \text{ GeV}$. The event is accepted as a Higgs candidate if $|m_{\gamma\gamma} - m_H| < 0.05 m_H$.

The numbers of events observed and expected in the full data sample at $\sqrt{s} = 189\text{--}209 \text{ GeV}$ are shown in Table 3 for several m_H hypotheses. The contamination from processes other than $e^+e^- \rightarrow \gamma\gamma(\gamma)$, as estimated from Monte Carlo simulations, is found to be negligible. The signal selection efficiency is in the range 25% – 30%, depending on m_H and \sqrt{s} .

4.2 The $e^+e^- \rightarrow e^+e^-H \rightarrow e^+e^-\gamma\gamma$ analysis

In the process $e^+e^- \rightarrow e^+e^-H$, the final state e^- and e^+ tend to escape detection at low polar angles, originating events with missing longitudinal momentum and missing mass. The selection requires two photon candidates from the $H \rightarrow \gamma\gamma$ decay in the central region of the detector. A kinematic fit is performed assuming the missing momentum to point in the beam pipe and the visible mass of the event to be consistent, within the experimental resolution, with the m_H hypothesis under investigation. The distribution of the χ^2 of the fit is shown in Figure 2b for $m_H = 130$ GeV. Events are accepted as Higgs candidates if $\chi^2 < 50 - 0.2 \text{ GeV}^{-1} \times m_H$. The dependence of the cut on m_H reflects the decrease of the background contribution for increasing values of m_H .

The numbers of events observed and expected in the full data sample at $\sqrt{s} = 189 - 209$ GeV are shown in Table 3 for several m_H hypotheses. The background comes from $e^+e^- \rightarrow \gamma\gamma(\gamma)$ events. The signal selection efficiency varies from 20% to 30%, with a smooth dependence on m_H and \sqrt{s} .

4.3 The $e^+e^- \rightarrow H\gamma \rightarrow Z\gamma\gamma$ analysis

Pre-selected hadronic events with two isolated high energy photons are considered for the $e^+e^- \rightarrow H\gamma \rightarrow Z\gamma\gamma$ analysis. Events are retained which have a recoiling mass, m_{rec} , calculated from the four-momenta of the two photons, compatible with m_Z : $80 \text{ GeV} < m_{rec} < 110 \text{ GeV}$. The hadronic system is clustered into two jets with the DURHAM [26] algorithm and a kinematic fit, in which the jet angles are fixed and the jet energies can vary, is performed to improve the resolution on the reconstructed Z-boson mass. Of the two possible combinations of two jets and a photon, the one is retained with mass, $m_{q\bar{q}\gamma}$, closer to the m_H hypothesis under investigation. The distribution of $m_{q\bar{q}\gamma}$ is shown in Figure 2c for $m_H = 150$ GeV. An event is considered as a Higgs candidate if $|m_{q\bar{q}\gamma} - m_H| < 15 \text{ GeV}$.

The numbers of events observed and expected in the data sample at $\sqrt{s} = 192 - 209$ GeV are shown in Table 3 for several m_H hypotheses. The signal selection efficiency is around 22%. The background is dominated by resonant $e^+e^- \rightarrow Z\gamma\gamma$ production (70%) with contributions from the $e^+e^- \rightarrow q\bar{q}(\gamma)$ process and four-fermion final states.

4.4 The $e^+e^- \rightarrow H\gamma \rightarrow WW^{(*)}\gamma$ analysis

The energy of the photon in the $e^+e^- \rightarrow H\gamma \rightarrow WW^{(*)}\gamma$ process depends on m_H as $E_\gamma^{rec}(m_H) = (s - m_H^2)/2\sqrt{s}$. Pre-selected hadronic events are retained if they have a photon with energy compatible with the m_H hypothesis under investigation, $E_\gamma^{rec}(m_H + 20 \text{ GeV}) < E_\gamma < E_\gamma^{rec}(m_H - 20 \text{ GeV})$. If multiple photon candidates are observed, the photon is retained which has an energy closest to $E_\gamma^{rec}(m_H)$. The rest of the event is clustered into four jets by means of the DURHAM algorithm.

A kinematic fit, in which the jet angles are fixed and the jet energies can vary, is performed to improve the resolution on the reconstructed W-boson mass. For $m_H > 2m_W$ both W bosons are on-shell and the constraint that both invariant jet-jet masses be compatible with m_W is included in the fit. For $m_H < 2m_W$ one of the W bosons is off-shell and only one of the invariant jet-jet masses is required to be compatible with m_W . The fit is repeated for all possible jet pairings and the pairing is chosen for which the χ^2 of the fit is minimal. An event is considered as a Higgs candidate if $\chi^2 < 6.0$ for the hypothesis $m_H < 2m_W$ or $\chi^2 < 15.0$ for $m_H > 2m_W$.

The invariant mass of the four-jet system, m_{qqqq} , estimates m_{H} . Its distribution is presented in Figure 2d for $m_{\text{H}} = 170$ GeV.

The numbers of events observed and expected in the data sample at $\sqrt{s} = 192 - 209$ GeV are shown in Table 3 for several m_{H} hypotheses. The signal selection efficiency is around 25%, for $150 \text{ GeV} < m_{\text{H}} < 170 \text{ GeV}$, decreasing to about 20% for masses out of this range. A small dependence on \sqrt{s} is observed. The background is dominated by the processes $e^+e^- \rightarrow \text{q}\bar{\text{q}}(\gamma)$ and $e^+e^- \rightarrow \text{W}^+\text{W}^-(\gamma)$, which is above 65% for $m_{\text{H}} > 150$ GeV.

5 Cross sections limits

The results of all the analyses agree with the Standard Model predictions and show no evidence for a Higgs boson with anomalous couplings in the m_{H} mass range under study. Upper limits on the product of the production cross sections and the corresponding decay branching fractions are derived [27] at the 95% confidence level (CL). The cross section of the $e^+e^- \rightarrow e^+e^-\text{H}$ process is proportional to the partial Higgs width into photons, $\Gamma(\text{H} \rightarrow \gamma\gamma)$, and limits are quoted on $\Gamma(\text{H} \rightarrow \gamma\gamma) \times \text{Br}(\text{H} \rightarrow \gamma\gamma)$.

In order to combine data sets at different \sqrt{s} values, a dependence of the type $\sigma^{AC}(\sqrt{s}) = \zeta \sigma^{SM}(\sqrt{s})$ is assumed for the cross section of anomalous Higgs production, σ^{AC} . The $e^+e^- \rightarrow \text{H}\gamma$ production cross section in the Standard Model, σ^{SM} , accounts for the dominant dependence on \sqrt{s} while ζ is a parameter which does not depend on \sqrt{s} . Limits on ζ are derived and interpreted as cross section limits at the luminosity-averaged centre-of-mass energy $\langle \sqrt{s} \rangle = 197.8$ GeV.

The cross section limits for the investigated processes are given in Figure 3 together with the expectations for non-zero values of the anomalous couplings.

6 Limits on anomalous couplings

6.1 Results from $e^+e^- \rightarrow \text{HZ}$ with $\text{H} \rightarrow \text{f}\bar{\text{f}}$ or $\text{H} \rightarrow \gamma\gamma$

The process $e^+e^- \rightarrow \text{HZ}$, with $\text{H} \rightarrow \text{f}\bar{\text{f}}$, studied in Reference 8, is sensitive to anomalous HZZ and HZ γ couplings in the Higgs production vertex. In addition, the process $e^+e^- \rightarrow \text{HZ}$ with $\text{H} \rightarrow \gamma\gamma$, object of the search for a fermiophobic Higgs [9], is sensitive to the H $\gamma\gamma$ coupling in the decay vertex.

Limits on the coupling ξ^2 are derived from the results of our search for the Standard Model Higgs boson [8]. They are obtained by interpreting ξ^2 as a scale factor of the Higgs production cross section and are shown in Figure 4. They include the systematic uncertainties on the search for the Standard Model Higgs boson [8].

The limits on the couplings d , d_B , Δg_1^Z and $\Delta\kappa_\gamma$ are extracted from the numbers of observed events, expected background and signal events reported in References 8 and 9. These limits are driven by the size of the deviations of the product $\sigma^{AC} \times \text{Br}^{AC}$ with respect to $\sigma^{SM} \times \text{Br}^{SM}$, where Br^{AC} and Br^{SM} denote the Higgs branching ratios in the presence of anomalous couplings and in the Standard Model respectively. The ratios $R = (\sigma^{AC} \times \text{Br}^{AC})/(\sigma^{SM} \times \text{Br}^{SM})$ are shown in Figure 5 for $\text{H} \rightarrow \text{f}\bar{\text{f}}$ and $\text{H} \rightarrow \gamma\gamma$, for $m_{\text{H}} = 100$ GeV.

The $\text{H} \rightarrow \text{f}\bar{\text{f}}$ and $\text{H} \rightarrow \gamma\gamma$ channels have different behaviours with respect to the parameters d and d_B , as these describe the H $\gamma\gamma$ coupling. The parameters Δg_1^Z and $\Delta\kappa_\gamma$ describe the

HZ γ and HZZ couplings and hence affect only the Higgs production vertex in the $e^+e^- \rightarrow \text{HZ}$ process. They give similar deviations for both the $\text{H} \rightarrow \text{ff}$ and $\text{H} \rightarrow \gamma\gamma$ channels.

6.2 One-dimensional limits

Figure 6 presents the limits on d , d_B , Δg_1^Z and $\Delta\kappa_\gamma$ as a function of m_{H} . A coupling at the time is considered, fixing the others to zero. Limits from the most sensitive channels are shown in addition to the combined results.

The region $m_{\text{H}} \lesssim \sqrt{s} - m_Z$ is excluded by the $e^+e^- \rightarrow \text{HZ}$ search for any value of the four couplings. The fermiophobic search $e^+e^- \rightarrow \text{HZ}$, with $\text{H} \rightarrow \gamma\gamma$, is sensitive to large values of d and d_B , for which there is an enhancement of the $\text{H} \rightarrow \gamma\gamma$ branching fraction. The standard search $e^+e^- \rightarrow \text{HZ}$, with $\text{H} \rightarrow \text{b}\bar{\text{b}}$ or $\tau^+\tau^-$, covers the region $d \approx d_B \approx 0$. A region for $m_{\text{H}} \sim 97$ GeV in the d vs. m_{H} plane of Figure 6a is not excluded due to an excess of events observed in the $e^+e^- \rightarrow \text{HZ}$ search [28].

The $e^+e^- \rightarrow \text{H}\gamma \rightarrow \gamma\gamma\gamma$ and $e^+e^- \rightarrow e^+e^-\text{H} \rightarrow e^+e^-\gamma\gamma$ channels have a large sensitivity if the $\text{H}\gamma\gamma$ coupling is large, *i.e.* when $d\sin^2\theta_W + d_B\cos^2\theta_W$ has a sizable value (Figures 6a and 6b). On the other hand, the $e^+e^- \rightarrow \text{H}\gamma \rightarrow \text{Z}\gamma\gamma$ process has a dominant role when the channel $\text{H} \rightarrow \gamma\gamma$ is suppressed, which occurs for the couplings Δg_1^Z and $\Delta\kappa_\gamma$ in the mass region $m_Z < m_{\text{H}} < 2m_W$ (Figures 6c and 6d).

The contribution from the $e^+e^- \rightarrow \text{H}\gamma \rightarrow \text{WW}^{(*)}\gamma$ process to the limits presented in Figures 6a and 6c is small and restricted to $m_{\text{H}} \sim 160$ GeV. This happens since a large decay width for $\text{H} \rightarrow \text{WW}^{(*)}$ corresponds to large values of d or Δg_1^Z which also imply large widths for the competing modes $\text{H} \rightarrow \gamma\gamma$ and $\text{H} \rightarrow \text{Z}\gamma$.

The sensitivity of the analysis degrades rapidly when m_{H} approaches the $2m_W$ threshold, where the $\text{H} \rightarrow \gamma\gamma$ and $\text{H} \rightarrow \text{Z}\gamma$ are no longer dominant, even in the presence of relatively large anomalous couplings.

Several sources of systematic uncertainties are investigated and their impact on the signal efficiency and background level is evaluated. The limited Monte Carlo statistics affects the signal by less than 2% and the background by 8% for the photonic channels and less than 4% for the hadronic channels. The accuracy of the cross section calculation for background processes adds less than 0.4% to the uncertainty in the background normalisation. The systematic uncertainty due to the selection procedure was estimated by varying the most important selection criteria and was found to be less than 1%. In particular, the effect of the limited knowledge of the energy scale of the electromagnetic calorimeter has a small impact in the limits.

The combined effect of the systematic uncertainties is included in the limits shown in Figure 6. It degrades the limits by at most 4%, slightly depending on the coupling and the Higgs mass hypothesis.

We verified that possible effects of angular dependence of the efficiency on the value of the anomalous couplings is negligible for the $e^+e^- \rightarrow \text{HZ}$ process. No such effects are expected for the $e^+e^- \rightarrow e^+e^-\text{H}$ and $e^+e^- \rightarrow \text{H}\gamma$ processes.

6.3 Two-dimensional limits

Assuming the absence of large anomalous WWZ and WW γ couplings, *i.e.* $\Delta g_1^Z = \Delta\kappa_\gamma = 0$ [29], the H $\gamma\gamma$ and HZ γ couplings are parametrized via the following subset of effective operators:

$$\mathcal{L}_{\text{eff}} = g_{\text{H}\gamma\gamma} \text{H}A_{\mu\nu}A^{\mu\nu} + g_{\text{HZ}\gamma}^{(2)} \text{H}A_{\mu\nu}Z^{\mu\nu} + h.c. \quad (10)$$

where the dependence of $g_{H\gamma\gamma}$ and $g_{HZ\gamma}^{(2)}$ on the d and d_B couplings is given by Equations 2 and 4. This Lagrangian is used to compute the maximal partial widths and branching fractions of the decays $H \rightarrow Z\gamma$ and $H \rightarrow \gamma\gamma$, allowed by the limits on d and d_B . The results are presented in Figure 7 for two different Higgs masses, in the region of interest for Higgs searches at future colliders. The results are consistent with the tree level Standard Model expectations $\Gamma(H \rightarrow Z\gamma) \approx \Gamma(H \rightarrow \gamma\gamma) \approx 0$.

References

- [1] S.L. Glashow, Nucl. Phys. **22** (1961) 579;
S. Weinberg, Phys. Rev. Lett. **19** (1967) 1264;
A. Salam, “Elementary Particle Theory”, Ed. N. Svartholm, Stockholm, Almqvist and Wiksell (1968), 367;
P.W. Higgs, Phys. Lett. **12** (1964) 132.
- [2] W. Buchmüller and D. Wyler, Nucl. Phys. **B 268** (1986) 621;
C.J.C. Burges and H.J. Schnitzer, Nucl. Phys. **B 228** (1983) 424;
C.N. Leung, S.T. Love and S. Rao, Z. Phys. **C 31** (1986) 433.
- [3] O.J.P. Éboli *et al.*, Phys. Lett. **B 434** (1998) 340;
M.C. González-García, Int. J. Mod. Phys. **A 14** (1999) 3121.
- [4] G.J. Gounaris, F.M. Renard and N.D. Vlachos, Nucl. Phys. **B 459** (1996) 51.
- [5] K. Hagiwara *et al.*, Nucl. Phys. **B 282** (1987) 253.
- [6] B. Grzadkowski and J. Wudka, Phys. Lett. **B 364** (1995) 49.
- [7] S. Alam, S. Dawson and R. Szalapski, Phys. Rev. **D 57** (1998) 1577.
- [8] L3 Collaboration, P. Achard *et al.*, Phys. Lett. **B 517** (2001) 319.
- [9] L3 Collaboration, P. Achard *et al.*, Phys. Lett. **B 534** (2002) 28.
- [10] L3 Collaboration, B. Adeva *et al.*, Nucl. Inst. Meth. **A 289** (1990) 35;
L3 Collaboration, O. Adriani *et al.*, Phys. Rep. **236** (1993) 1;
J.A. Bakken *et al.*, Nucl. Inst. Meth. **A 275** (1989) 81;
O. Adriani *et al.*, Nucl. Inst. Meth. **A 302** (1991) 53;
B. Adeva *et al.*, Nucl. Inst. Meth. **A 323** (1992) 109;
K. Deiters *et al.*, Nucl. Inst. Meth. **A 323** (1992) 162;
M. Chemarin *et al.*, Nucl. Inst. Meth. **A 349** (1994) 345;
G. Basti *et al.*, Nucl. Inst. Meth. **A 374** (1996) 293;
A. Adam *et al.*, Nucl. Inst. Meth. **A 383** (1996) 342.
- [11] L3 Collaboration, M. Acciarri *et al.*, Phys. Lett. **B 489** (2000) 102.
- [12] DELPHI Collaboration, P. Abreu *et al.*, Phys. Lett. **B 458** (1999) 431.
- [13] ALEPH Collaboration, A. Heister *et al.*, Phys. Lett. **B 544** (2002) 16;
DELPHI Collaboration, P. Abreu *et al.*, Phys. Lett. **B 507** (2001) 89;
L3 Collaboration, P. Achard *et al.*, Phys. Lett. **B 568** (2003) 191;
OPAL Collaboration, G. Abbiendi *et al.*, Phys. Lett. **B 544** (2002) 44.

- [14] F.A. Berends and R. Kleiss, Nucl. Phys. **B 260** (1985) 32.
- [15] E. Barberio and Z. Wąs, Comp. Phys. Comm. **79** (1994) 291.
- [16] F.L. Linde, “Charm Production in Two-Photon Collisions”, Ph.D. Thesis, Rijksuniversiteit Leiden 1988.
- [17] K. Hagiwara and M.L. Stong, Z. Phys. **C 62** (1994) 99.
- [18] K. Hagiwara, R. Szalapski and D. Zeppenfeld, Phys. Lett. **B 318** (1993) 155.
- [19] J.C. Romao and S. Andringa, Eur. Phys. J. **C7** (1999) 631.
- [20] GGG Monte Carlo; F. A. Berends and R. Kleiss, Nucl. Phys. **B 186** (1981) 22.
- [21] KK2f version 4.12; S. Jadach, B.F.L. Ward and Z. Wąs, Comp. Phys. Comm. **130** (2000) 260.
- [22] PYTHIA version 5.722; T. Sjöstrand, preprint CERN-TH/7112/93, (1993), revised 1995; T. Sjöstrand, Comp. Phys. Comm. **82** (1994) 74.
- [23] KORALW version 1.33; M. Skrzypek *et al.*, Comp. Phys. Comm. **94** (1996) 216.
- [24] EXCALIBUR version 1.11; F.A. Berends, R. Pittau and R. Kleiss, Comp. Phys. Comm. **85** (1995) 437.
- [25] GEANT version 3.15 is used; R. Brun *et al.*, preprint CERN DD/EE/84-1 (1985), revised 1987. The GHEISHA program (H. Fesefeldt, RWTH Aachen Report PITHA 85/02, 1985) is used to simulate hadronic interactions.
- [26] S. Bethke *et al.*, Nucl. Phys. **B 370** (1992) 310.
- [27] ALEPH, DELPHI, L3 and OPAL Collaborations, The LEP Working group for the Higgs Boson Searches, Phys. Lett. **B 565** (2003) 61.
- [28] L3 Collaboration, M. Acciarri *et al.*, Phys. Lett. **B 508** (2001) 225.
- [29] L3 Collaboration, P. Achard *et al.*, preprint hep-ex/0402036 (2003), to appear in Physics Letters.

The L3 Collaboration:

P.Achard,²⁰ O.Adriani,¹⁷ M.Aguilar-Benitez,²⁵ J.Alcaraz,²⁵ G.Alemanni,²³ J.Allaby,¹⁸ A.Aloisio,²⁹ M.G.Alvigi,²⁹ H.Anderhub,⁴⁹ V.P.Andreev,^{6,34} F.Anselmo,⁸ A.Arefiev,²⁸ T.Azemoon,³ T.Aziz,⁹ P.Bagnaia,³⁹ A.Bajo,²⁵ G.Baksay,²⁶ L.Baksay,²⁶ S.V.Baldew,² S.Banerjee,⁹ Sw.Banerjee,⁴ A.Barczyk,^{49,47} R.Barillère,¹⁸ P.Bartalini,²³ M.Basile,⁸ N.Batalova,⁴⁶ R.Battiston,³³ A.Bay,²³ F.Becattini,¹⁷ U.Becker,¹³ F.Behner,⁴⁹ L.Bellucci,¹⁷ R.Berbeco,³ J.Berdugo,²⁵ P.Berges,¹³ B.Bertucci,³³ B.L.Betev,⁴⁹ M.Biasini,³³ M.Biglietti,²⁹ A.Biland,⁴⁹ J.J.Blaising,⁴ S.C.Blyth,³⁵ G.J.Bobbink,² A.Böhm,¹ L.Boldizar,¹² B.Borgia,³⁹ S.Bottai,¹⁷ D.Bourilkov,⁴⁹ M.Bourquin,²⁰ S.Braccini,²⁰ J.G.Branson,⁴¹ F.Brochu,⁴ J.D.Burger,¹³ W.J.Burger,³³ X.D.Cai,¹³ M.Capell,¹³ G.Cara Romeo,⁸ G.Carlino,²⁹ A.Cartacci,¹⁷ J.Casaus,²⁵ F.Cavallari,³⁹ N.Cavallo,³⁶ C.Cecchi,³³ M.Cerrada,²⁵ M.Chamizo,²⁰ Y.H.Chang,⁴⁴ M.Chemarin,²⁴ A.Chen,⁴⁴ G.Chen,⁷ G.M.Chen,⁷ H.F.Chen,²² H.S.Chen,⁷ G.Chiefari,²⁹ L.Cifarelli,⁴⁰ F.Cindolo,⁸ I.Clare,¹³ R.Clare,³⁸ G.Coignet,⁴ N.Colino,²⁵ S.Costantini,³⁹ B.de la Cruz,²⁵ S.Cucciarelli,³³ J.A.van Dalen,³¹ R.de Asmundis,²⁹ P.Déglon,²⁰ J.Debreczeni,¹² A.Degré,⁴ K.Dehmelt,²⁶ K.Deiters,⁴⁷ D.della Volpe,²⁹ E.Delmeire,²⁰ P.Denes,³⁷ F.DeNotaristefani,³⁹ A.De Salvo,⁴⁹ M.Diemoz,³⁹ M.Dierckxsens,² C.Dionisi,³⁹ M.Dittmar,⁴⁹ A.Doria,³⁹ M.T.Dova,^{10,‡} P.Duchesneau,⁴ M.Duda,¹ B.Echenard,²⁰ A.Eline,¹⁸ A.El Hage,¹ H.El Mamouni,²⁴ A.Engler,³⁵ F.J.Eppling,¹³ P.Extermann,²⁰ M.A.Falagan,²⁵ S.Falciano,³⁹ A.Favara,³² J.Fay,²⁴ O.Fedin,³⁴ M.Felcini,⁴⁹ T.Ferguson,³⁵ H.Fesefeldt,¹ E.Fiandrini,³³ J.H.Field,²⁰ F.Filthaut,³¹ P.H.Fisher,¹³ W.Fisher,³⁷ I.Fisk,⁴¹ G.Forconi,¹³ K.Freundreich,⁴⁹ C.Furetta,²⁷ Yu.Galaktionov,^{28,13} S.N.Ganguli,⁹ P.Garcia-Abia,²⁵ M.Gataullin,³² S.Gentile,³⁹ S.Giagu,³⁹ Z.F.Gong,²² G.Grenier,²⁴ O.Grimm,⁴⁹ M.W.Gruenewald,¹⁶ M.Guida,⁴⁰ R.van Gulik,² V.K.Gupta,³⁷ A.Gurtu,⁹ L.J.Gutay,⁴⁶ D.Haas,⁵ D.Hatzifotiadou,⁸ T.Hebbeker,¹ A.Hervé,¹⁸ J.Hirschfelder,³⁵ H.Hofer,⁴⁹ M.Hohlmann,²⁶ G.Holzner,⁴⁹ S.R.Hou,⁴⁴ Y.Hu,³¹ B.N.Jin,⁷ L.W.Jones,³ P.de Jong,² I.Josa-Mutuberría,²⁵ M.Kaur,¹⁴ M.N.Kienzle-Focacci,²⁰ J.K.Kim,⁴³ J.Kirkby,¹⁸ W.Kittel,³¹ A.Klimentov,^{13,28} A.C.König,³¹ M.Kopal,⁴⁶ V.Koutsenko,^{13,28} M.Kräber,⁴⁹ R.W.Kraemer,³⁵ A.Krüger,⁴⁸ A.Kunin,¹³ P.Ladron de Guevara,²⁵ I.Laktineh,²⁴ G.Landi,¹⁷ M.Lebeau,¹⁸ A.Lebedev,¹³ P.Lebrun,²⁴ P.Lecomte,⁴⁹ P.Lecoq,¹⁸ P.Le Coultre,⁴⁹ J.M.Le Goff,¹⁸ R.Leiste,⁴⁸ M.Levtchenko,²⁷ P.Levtchenko,³⁴ C.Li,²² S.Likhoded,⁴⁸ C.H.Lin,⁴⁴ W.T.Lin,⁴⁴ F.L.Linde,²⁹ L.Lista,²⁹ Z.A.Liu,⁷ W.Lohmann,⁴⁸ E.Longo,³⁹ Y.S.Lu,⁷ C.Luci,³⁹ L.Luminari,³⁹ W.Lustermann,⁴⁹ W.G.Ma,²² L.Malgeri,²⁰ A.Malinin,²⁸ C.Maña,²⁵ J.Mans,³⁷ J.P.Martin,²⁴ F.Marzano,³⁹ K.Mazumdar,⁹ R.R.McNeil,¹⁶ S.Mele,^{18,29} L.Merola,²⁹ M.Meschini,¹⁷ W.J.Metzger,³¹ A.Mihul,¹¹ H.Milcent,¹⁸ G.Mirabelli,³⁹ J.Mnich,¹ G.B.Mohanty,⁹ G.S.Muanza,²⁴ A.J.M.Muijs,² B.Musicar,⁴¹ M.Musy,³⁹ S.Nagy,¹⁵ S.Natale,²⁰ M.Napolitano,²⁹ F.Nessi-Tedaldi,⁴⁹ H.Newman,³² A.Nisati,³⁹ T.Novak,³¹ H.Nowak,⁴⁸ R.Ofierzynski,⁴⁹ G.Organtini,³⁹ I.Pal,⁴⁶ C.Palomares,²⁵ P.Paolucci,²⁹ R.Paramatti,³⁹ G.Passaleva,¹⁷ S.Patricelli,²⁹ T.Paul,¹⁰ M.Pauluzzi,³³ C.Paus,¹³ F.Pauss,⁴⁹ M.Pedace,³⁹ S.Pensotti,²⁷ D.Perret-Gallix,⁴ B.Petersen,³¹ D.Piccolo,²⁹ F.Pierella,⁸ M.Pioppi,³³ P.A.Piroué,³⁷ E.Pistolessi,²⁷ V.Plyaskin,²⁸ M.Pohl,²⁰ V.Pojidaev,¹⁷ J.Pothier,¹⁸ D.Prokofiev,³⁴ J.Quartieri,⁴⁰ G.Rahal-Callot,⁴⁹ M.A.Rahaman,⁹ P.Raics,¹⁵ N.Raja,⁹ R.Ramelli,⁴⁹ P.G.Rancoita,²⁷ R.Ranieri,¹⁷ A.Raspereza,⁴⁸ P.Razis,³⁰ D.Ren,⁴⁹ M.Rescigno,³⁹ S.Reucroft,¹⁰ S.Riemann,⁴⁸ K.Riles,³ B.P.Roe,³ L.Romero,²⁵ A.Rosca,⁴⁸ C.Rosemann,¹ C.Rosenbleck,¹ S.Rosier-Lees,⁴ S.Roth,¹ J.A.Rubio,¹⁸ G.Ruggiero,¹⁷ H.Rykaczewski,⁴⁹ A.Sakharov,⁴⁹ S.Saremi,⁶ S.Sarkar,³⁹ J.Salicio,¹⁸ E.Sanchez,²⁵ C.Schäfer,¹⁸ V.Schegelsky,³⁴ H.Schopper,²¹ D.J.Schotanus,³¹ C.Sciacca,²⁹ L.Servoli,³³ S.Shevchenko,³² N.Shivarov,⁴² V.Shoutko,¹³ E.Shumilov,²⁸ A.Shvorob,³² D.Son,⁴³ C.Souga,²⁴ P.Spillantini,¹⁷ M.Steuer,¹³ D.P.Stickland,³⁷ B.Stoyanov,⁴² A.Straessner,²⁰ K.Sudhakar,⁹ G.Sultanov,⁴² L.Z.Sun,²² S.Sushkov,¹ H.Suter,⁴⁹ J.D.Swain,¹⁰ Z.Szillasi,^{26,¶} X.W.Tang,⁷ P.Tarjan,¹⁵ L.Tauscher,⁵ L.Taylor,¹⁰ B.Tellili,²⁴ D.Teyssier,²⁴ C.Timmermans,³¹ Samuel C.C.Ting,¹³ S.M.Ting,¹³ S.C.Tonwar,⁹ J.Tóth,¹² C.Tully,³⁷ K.L.Tung,⁷ J.Ulbricht,⁴⁹ E.Valente,³⁹ R.T.Van de Walle,³¹ R.Vasquez,⁴⁶ V.Veszpremi,²⁶ G.Vesztergombi,¹² I.Vetlitsky,²⁸ D.Vicinanza,⁴⁰ G.Viertel,⁴⁹ S.Villa,³⁸ M.Vivargent,⁴ S.Vlachos,⁵ I.Vodopianov,²⁶ H.Vogel,³⁵ H.Vogt,⁴⁸ I.Vorobiev,^{35,28} A.A.Vorobyov,³⁴ M.Wadhwa,⁵ Q.Wang,³¹ X.L.Wang,²² Z.M.Wang,²² M.Weber,¹⁸ H.Wilkins,³¹ S.Wynhof,³⁷ L.Xia,³² Z.Z.Xu,²² J.Yamamoto,³ B.Z.Yang,²² C.G.Yang,⁷ H.J.Yang,³ M.Yang,⁷ S.C.Yeh,⁴⁵ An.Zalite,³⁴ Yu.Zalite,³⁴ Z.P.Zhang,²² J.Zhao,²² G.Y.Zhu,⁷ R.Y.Zhu,³² H.L.Zhuang,⁷ A.Zichichi,^{8,18,19} B.Zimmermann,⁴⁹ M.Zöller,¹

- 1 III. Physikalisches Institut, RWTH, D-52056 Aachen, Germany[§]
 - 2 National Institute for High Energy Physics, NIKHEF, and University of Amsterdam, NL-1009 DB Amsterdam, The Netherlands
 - 3 University of Michigan, Ann Arbor, MI 48109, USA
 - 4 Laboratoire d'Annecy-le-Vieux de Physique des Particules, LAPP,IN2P3-CNRS, BP 110, F-74941 Annecy-le-Vieux CEDEX, France
 - 5 Institute of Physics, University of Basel, CH-4056 Basel, Switzerland
 - 6 Louisiana State University, Baton Rouge, LA 70803, USA
 - 7 Institute of High Energy Physics, IHEP, 100039 Beijing, China[△]
 - 8 University of Bologna and INFN-Sezione di Bologna, I-40126 Bologna, Italy
 - 9 Tata Institute of Fundamental Research, Mumbai (Bombay) 400 005, India
 - 10 Northeastern University, Boston, MA 02115, USA
 - 11 Institute of Atomic Physics and University of Bucharest, R-76900 Bucharest, Romania
 - 12 Central Research Institute for Physics of the Hungarian Academy of Sciences, H-1525 Budapest 114, Hungary[‡]
 - 13 Massachusetts Institute of Technology, Cambridge, MA 02139, USA
 - 14 Panjab University, Chandigarh 160 014, India
 - 15 KLTE-ATOMKI, H-4010 Debrecen, Hungary[¶]
 - 16 Department of Experimental Physics, University College Dublin, Belfield, Dublin 4, Ireland
 - 17 INFN Sezione di Firenze and University of Florence, I-50125 Florence, Italy
 - 18 European Laboratory for Particle Physics, CERN, CH-1211 Geneva 23, Switzerland
 - 19 World Laboratory, FBLJA Project, CH-1211 Geneva 23, Switzerland
 - 20 University of Geneva, CH-1211 Geneva 4, Switzerland
 - 21 University of Hamburg, D-22761 Hamburg, Germany
 - 22 Chinese University of Science and Technology, USTC, Hefei, Anhui 230 029, China[△]
 - 23 University of Lausanne, CH-1015 Lausanne, Switzerland
 - 24 Institut de Physique Nucléaire de Lyon, IN2P3-CNRS, Université Claude Bernard, F-69622 Villeurbanne, France
 - 25 Centro de Investigaciones Energéticas, Medioambientales y Tecnológicas, CIEMAT, E-28040 Madrid, Spain^b
 - 26 Florida Institute of Technology, Melbourne, FL 32901, USA
 - 27 INFN-Sezione di Milano, I-20133 Milan, Italy
 - 28 Institute of Theoretical and Experimental Physics, ITEP, Moscow, Russia
 - 29 INFN-Sezione di Napoli and University of Naples, I-80125 Naples, Italy
 - 30 Department of Physics, University of Cyprus, Nicosia, Cyprus
 - 31 University of Nijmegen and NIKHEF, NL-6525 ED Nijmegen, The Netherlands
 - 32 California Institute of Technology, Pasadena, CA 91125, USA
 - 33 INFN-Sezione di Perugia and Università Degli Studi di Perugia, I-06100 Perugia, Italy
 - 34 Nuclear Physics Institute, St. Petersburg, Russia
 - 35 Carnegie Mellon University, Pittsburgh, PA 15213, USA
 - 36 INFN-Sezione di Napoli and University of Potenza, I-85100 Potenza, Italy
 - 37 Princeton University, Princeton, NJ 08544, USA
 - 38 University of California, Riverside, CA 92521, USA
 - 39 INFN-Sezione di Roma and University of Rome, "La Sapienza", I-00185 Rome, Italy
 - 40 University and INFN, Salerno, I-84100 Salerno, Italy
 - 41 University of California, San Diego, CA 92093, USA
 - 42 Bulgarian Academy of Sciences, Central Lab. of Mechatronics and Instrumentation, BU-1113 Sofia, Bulgaria
 - 43 The Center for High Energy Physics, Kyungpook National University, 702-701 Taegu, Republic of Korea
 - 44 National Central University, Chung-Li, Taiwan, China
 - 45 Department of Physics, National Tsing Hua University, Taiwan, China
 - 46 Purdue University, West Lafayette, IN 47907, USA
 - 47 Paul Scherrer Institut, PSI, CH-5232 Villigen, Switzerland
 - 48 DESY, D-15738 Zeuthen, Germany
 - 49 Eidgenössische Technische Hochschule, ETH Zürich, CH-8093 Zürich, Switzerland
- § Supported by the German Bundesministerium für Bildung, Wissenschaft, Forschung und Technologie.
‡ Supported by the Hungarian OTKA fund under contract numbers T019181, F023259 and T037350.
¶ Also supported by the Hungarian OTKA fund under contract number T026178.
^b Supported also by the Comisión Interministerial de Ciencia y Tecnología.
[‡] Also supported by CONICET and Universidad Nacional de La Plata, CC 67, 1900 La Plata, Argentina.
[△] Supported by the National Natural Science Foundation of China.

Production mechanism	Decay mode			
	$H \rightarrow \gamma\gamma$	$H \rightarrow Z\gamma$	$H \rightarrow WW^{(*)}$	$H \rightarrow f\bar{f}$
$e^+e^- \rightarrow H\gamma$	3γ	$2\gamma + 2\text{ jets}$	$1\gamma + 4\text{ jets}$	$1\gamma + b\bar{b}$ [11]
$e^+e^- \rightarrow He^+e^-$	$2\gamma + \cancel{p}$	–	–	$b\bar{b} + \cancel{p}$ [11]
$e^+e^- \rightarrow HZ$	$2\gamma + f\bar{f}$ [9]	–	–	$f\bar{f}f'\bar{f}'$ [8]

Table 1: Experimental signatures for the search for anomalous couplings in the Higgs sector. The symbol \cancel{p} denotes missing energy and momentum. Searches in the $e^+e^- \rightarrow H\gamma \rightarrow b\bar{b}\gamma$ and $e^+e^- \rightarrow e^+e^-H \rightarrow e^+e^-b\bar{b}$ channels are only performed at $\sqrt{s} = 189$ GeV [11].

\sqrt{s} (GeV)	188.6	191.6	195.5	199.5	201.7	204.8	206.6
\mathcal{L} (pb^{-1})	176.8	28.8	82.4	67.6	36.1	74.7	135.6

Table 2: Average centre-of-mass energy and integrated luminosity of the data samples used for the search for anomalous couplings in the Higgs sector.

m_H	$e^+e^- \rightarrow$											
	$H\gamma \rightarrow \gamma\gamma\gamma$			$e^+e^-H \rightarrow e^+e^-\gamma\gamma$			$H\gamma \rightarrow Z\gamma\gamma$			$H\gamma \rightarrow WW^{(*)}\gamma$		
	N_D	N_B	$\epsilon(\%)$	N_D	N_B	$\epsilon(\%)$	N_D	N_B	$\epsilon(\%)$	N_D	N_B	$\epsilon(\%)$
70	1	3.5	23.4	0	0.0	19.5	–	–	–	–	–	–
90	2	2.7	25.8	6	1.7	24.2	–	–	–	–	–	–
110	3	3.1	26.9	9	4.9	28.5	68	72.8	22.7	–	–	–
130	2	2.4	28.7	11	10.9	30.4	15	18.2	22.4	10	11.5	18.0
150	4	4.0	28.8	19	19.9	31.9	9	14.4	24.1	22	22.8	25.5
170	9	9.3	28.2	38	49.7	32.4	31	41.0	25.6	72	74.7	26.8
190	3	8.9	22.9	24	29.5	30.1	96	101.0	22.5	113	107.3	19.5

Table 3: Numbers of observed, N_D , and expected, N_B , events and signal selection efficiencies, ϵ , for different analysis channels and values of the Higgs mass. Centre-of-mass energies in the range $189 \text{ GeV} < \sqrt{s} < 209 \text{ GeV}$ are considered for the $e^+e^- \rightarrow H\gamma \rightarrow \gamma\gamma\gamma$ and $e^+e^- \rightarrow e^+e^-H \rightarrow e^+e^-\gamma\gamma$ channels, while the $e^+e^- \rightarrow H\gamma \rightarrow Z\gamma\gamma$ and $e^+e^- \rightarrow H\gamma \rightarrow WW^{(*)}\gamma$ channels are analysed in the $192 \text{ GeV} < \sqrt{s} < 209 \text{ GeV}$ range.

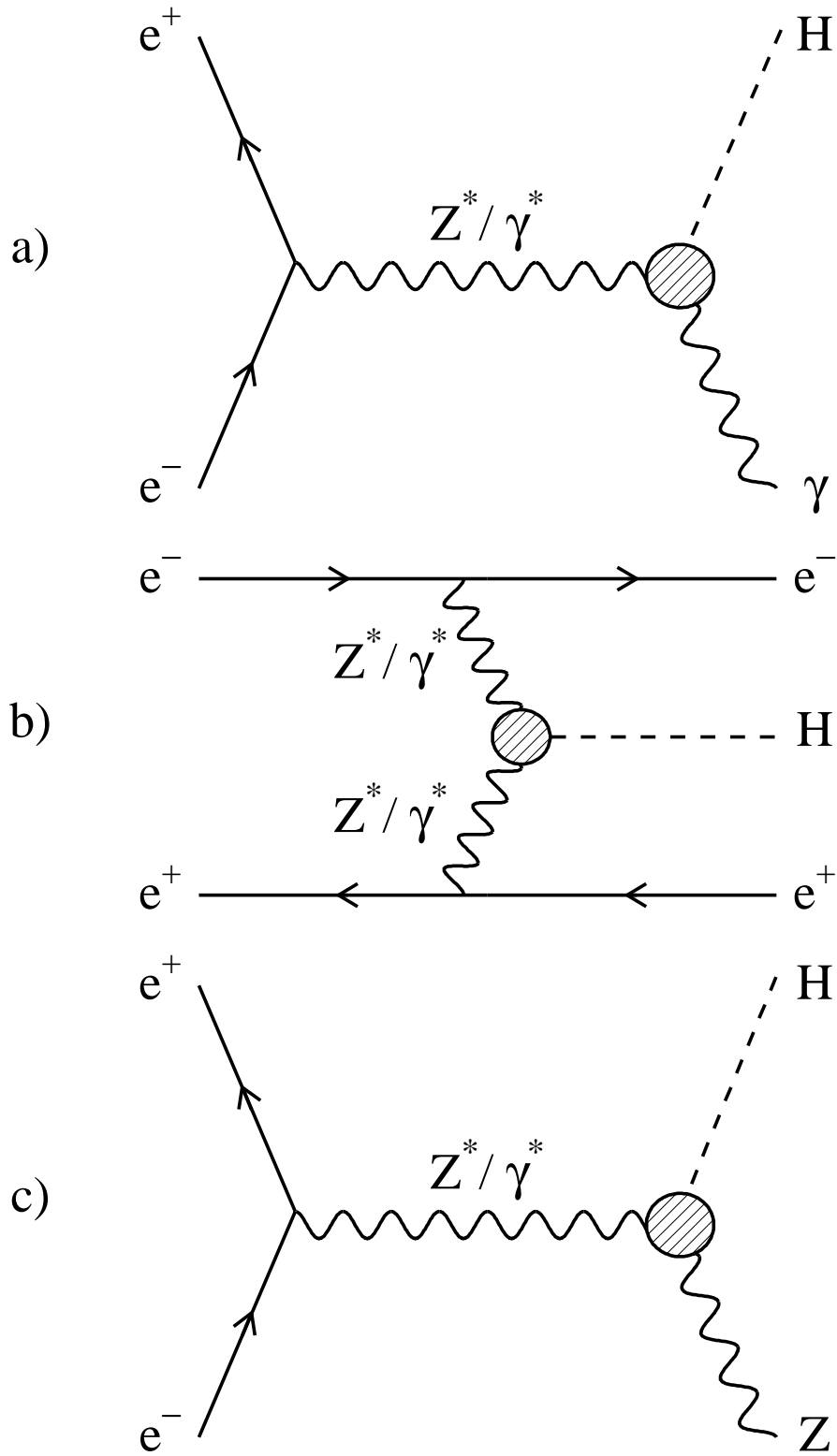


Figure 1: Relevant production processes in the search for anomalous couplings in the Higgs sector at LEP: a) $e^+e^- \rightarrow H\gamma$, b) $e^+e^- \rightarrow e^+e^-H$ and c) $e^+e^- \rightarrow HZ$.

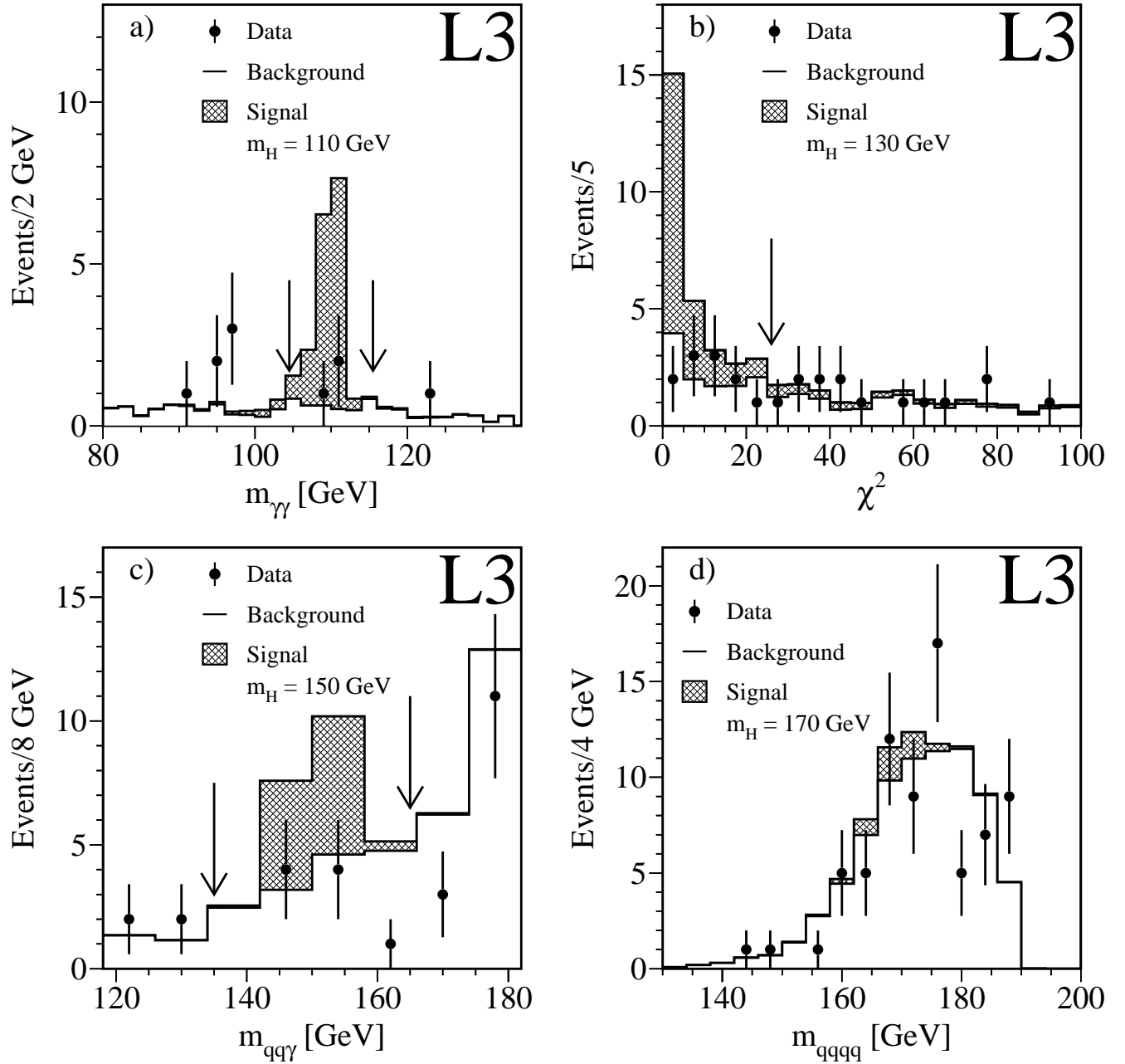


Figure 2: Distributions of the final discriminant variables for a) the $e^+e^- \rightarrow \gamma\gamma\gamma$ channel: the mass, $m_{\gamma\gamma}$, of the two-photon system; b) the $e^+e^- \rightarrow e^+e^-\gamma\gamma$ channel: the χ^2 of the constrained fit; c) the $e^+e^- \rightarrow Z\gamma\gamma$ channel: the mass, $m_{qq\gamma}$, of the system of the two-jets and a photon and d) the $e^+e^- \rightarrow WW^{(*)}\gamma$ channel: the mass, m_{qqqq} , of the hadronic system. The points represent the data, the open histograms the background and the hatched histograms the Higgs signal with an arbitrary cross section of 0.1 pb. The Higgs mass hypotheses indicated in the figures are considered. The arrows indicate the values of the cuts.

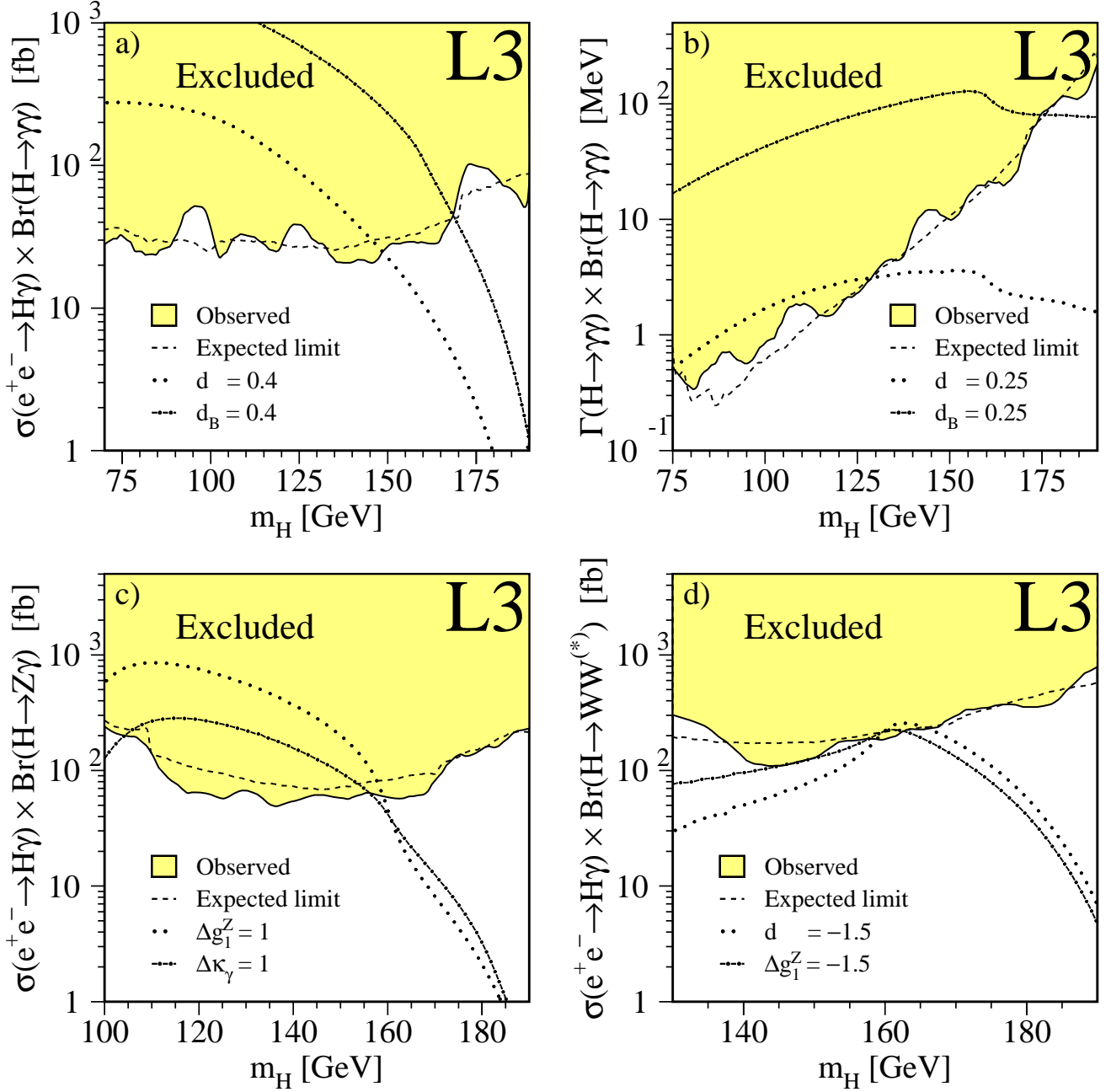


Figure 3: Upper limits at 95% CL as a function of the Higgs mass on: a) $\sigma(e^+e^- \rightarrow H\gamma) \times \text{Br}(H \rightarrow \gamma\gamma)$; b) $\Gamma(H \rightarrow \gamma\gamma) \times \text{Br}(H \rightarrow \gamma\gamma)$; c) $\sigma(e^+e^- \rightarrow H\gamma) \times \text{Br}(H \rightarrow Z\gamma)$; d) $\sigma(e^+e^- \rightarrow H\gamma) \times \text{Br}(H \rightarrow WW^{(*)})$. The dashed line indicates the expected limit in the absence of a signal. Predictions for non-zero values of the anomalous couplings are also shown.

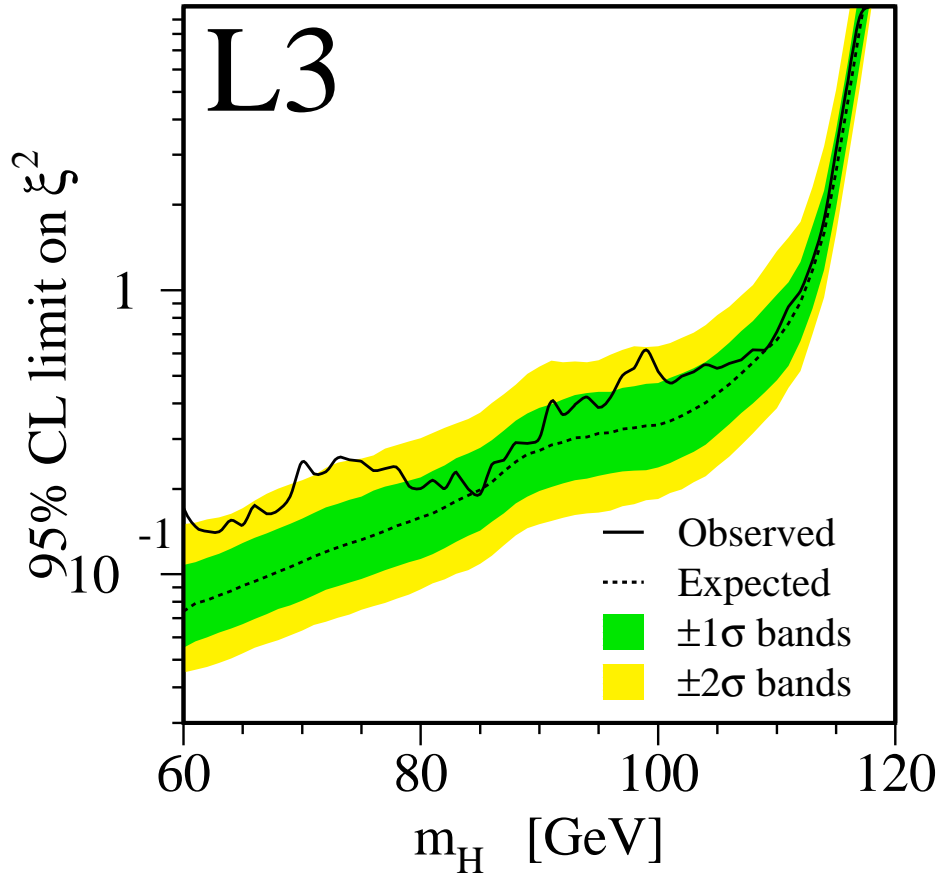


Figure 4: The 95% CL upper bound on the anomalous coupling ξ^2 as a function of the Higgs mass, as obtained from the results of the search for the Standard Model Higgs boson [8]. The dashed line indicates the expected limit in the absence of a signal. The dark and light shaded bands around the expected line correspond to the 68.3% and 95.4% probability bands, denoted by 1σ and 2σ respectively.

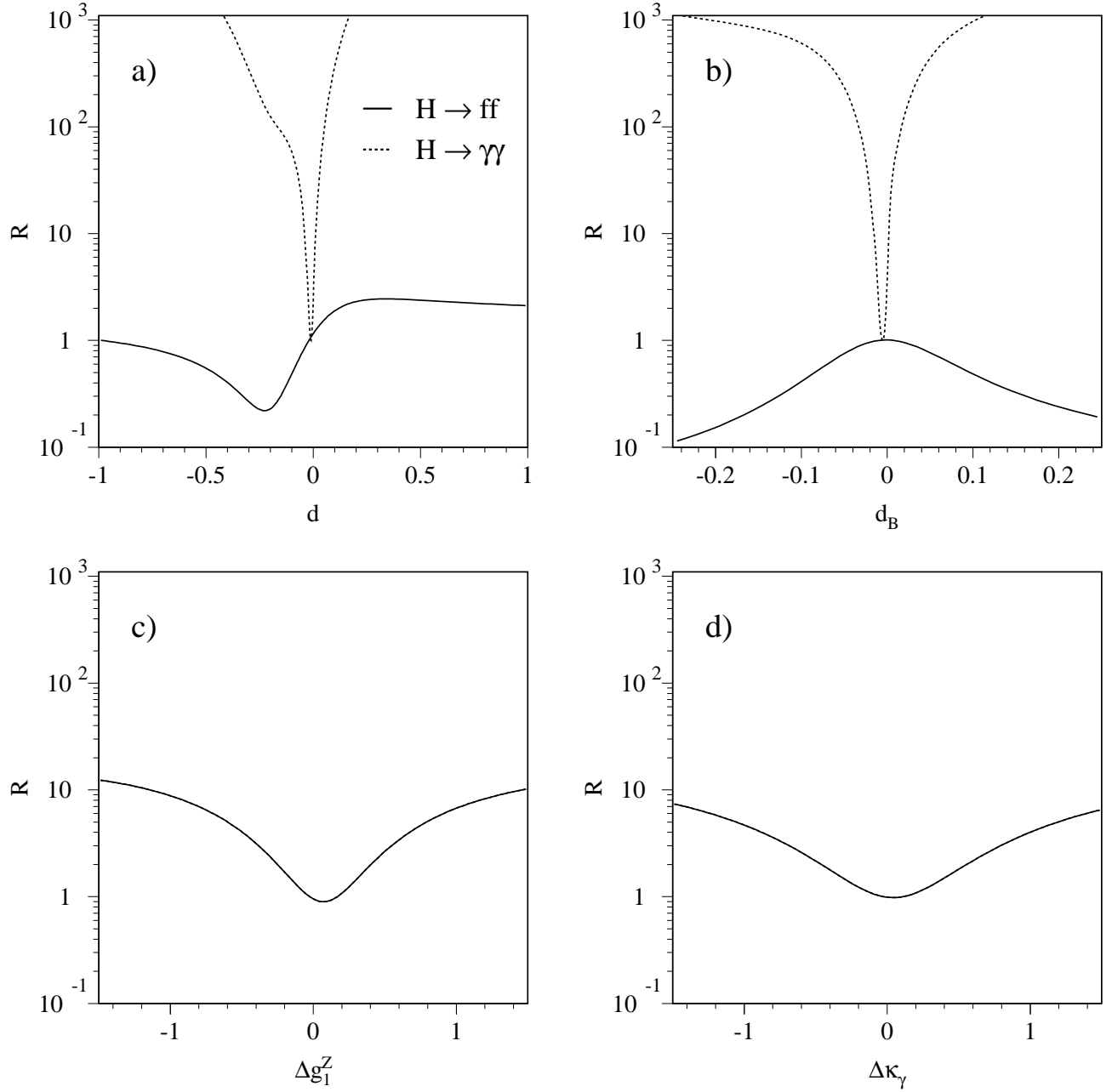


Figure 5: The theoretical predictions for the ratios $R = (\sigma^{AC} \times \text{Br}^{AC}) / (\sigma^{SM} \times \text{Br}^{SM})$ for the $e^+e^- \rightarrow HZ$ channel for the couplings a) d , b) d_B , c) Δg_1^Z and d) $\Delta \kappa_\gamma$. The solid line corresponds to the decay $H \rightarrow f\bar{f}$ and the dashed line to $H \rightarrow \gamma\gamma$. The predictions refer to $m_H = 100$ GeV. The ratios for the two decay modes coincide for Δg_1^Z and $\Delta \kappa_\gamma$.

Exclusion (95% CL):

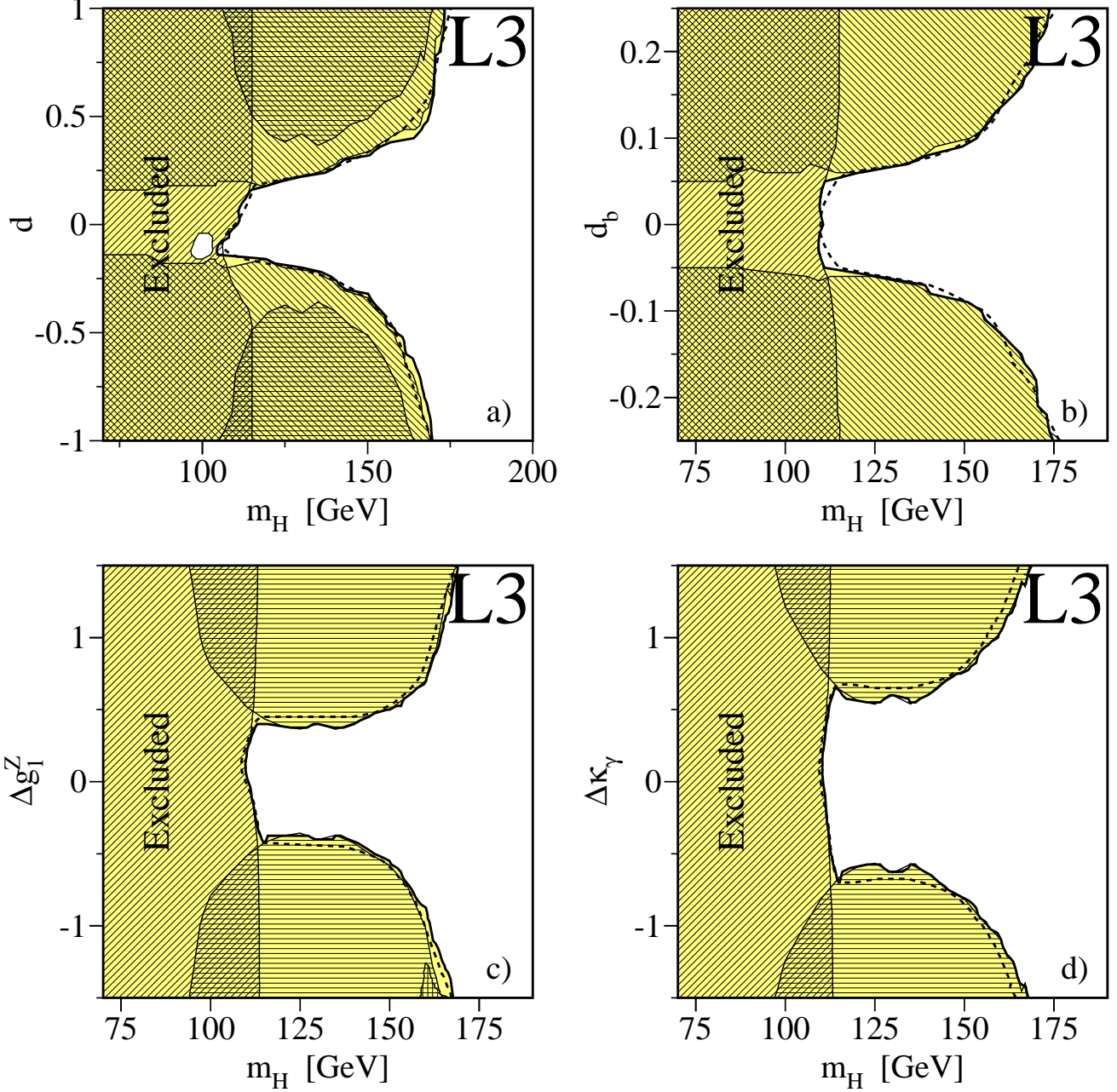
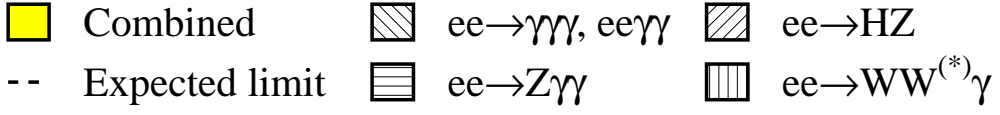


Figure 6: Regions excluded at 95% CL as a function of the Higgs mass for the anomalous couplings: a) d , b) d_B , c) Δg_1^Z and d) $\Delta \kappa_\gamma$. The limits on each coupling are obtained under the assumption that the other three couplings are equal to zero. The dashed line indicates the expected limit in the absence of a signal. The different hatched regions show the limits obtained by the most sensitive analyses: $e^+e^- \rightarrow H\gamma \rightarrow \gamma\gamma\gamma$, $e^+e^- \rightarrow e^+e^-H \rightarrow e^+e^-\gamma\gamma$, $e^+e^- \rightarrow H\gamma \rightarrow Z\gamma\gamma$, $e^+e^- \rightarrow HZ$ and $e^+e^- \rightarrow H\gamma \rightarrow WW^{(*)}\gamma$.

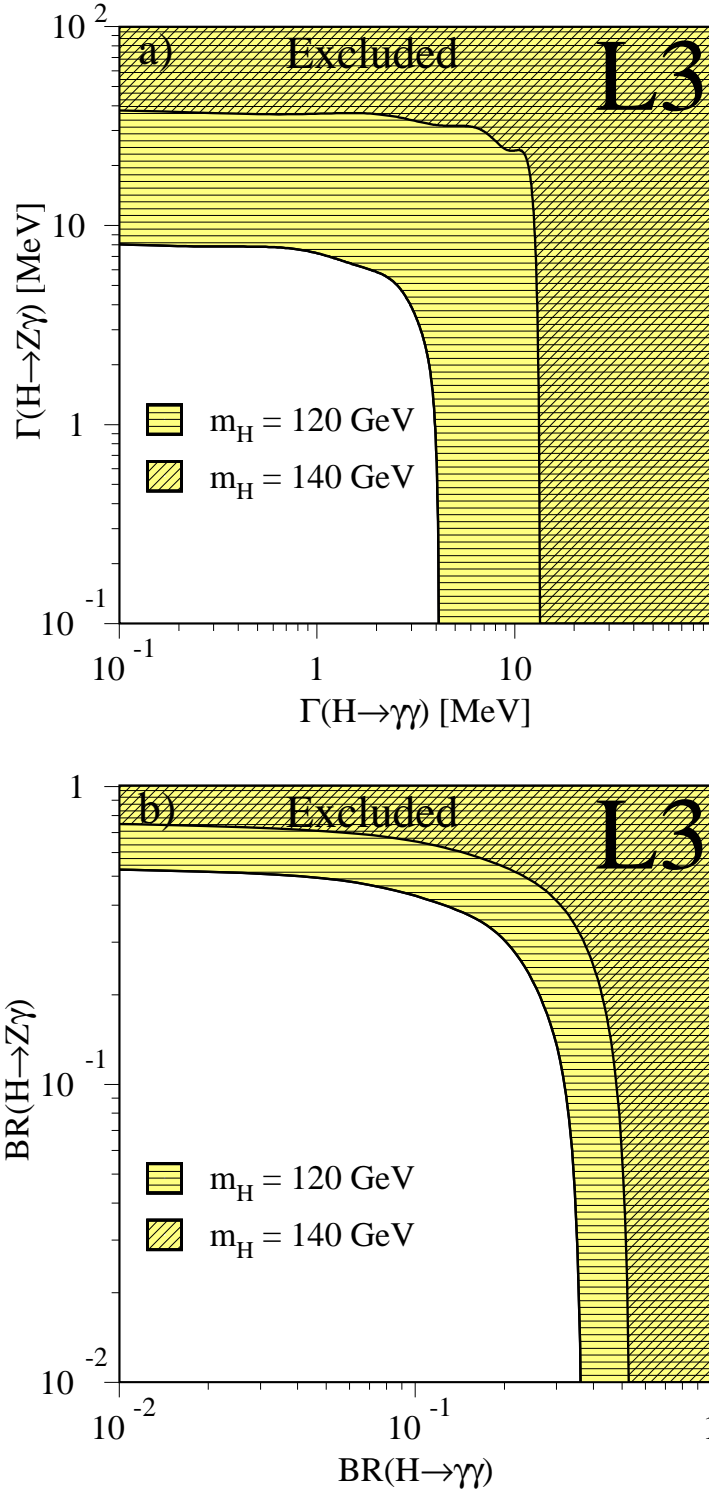


Figure 7: Regions excluded at 95% CL for: a) the partial widths $\Gamma(\text{H} \rightarrow \text{Z}\gamma)$ vs. $\Gamma(\text{H} \rightarrow \gamma\gamma)$ and b) the branching fractions $\text{Br}(\text{H} \rightarrow \text{Z}\gamma)$ vs. $\text{Br}(\text{H} \rightarrow \gamma\gamma)$ in presence of the d and d_B anomalous couplings. Two values of the Higgs boson mass are considered. The results are consistent with the tree level Standard Model expectations $\Gamma(\text{H} \rightarrow \text{Z}\gamma) \approx \Gamma(\text{H} \rightarrow \gamma\gamma) \approx 0$.